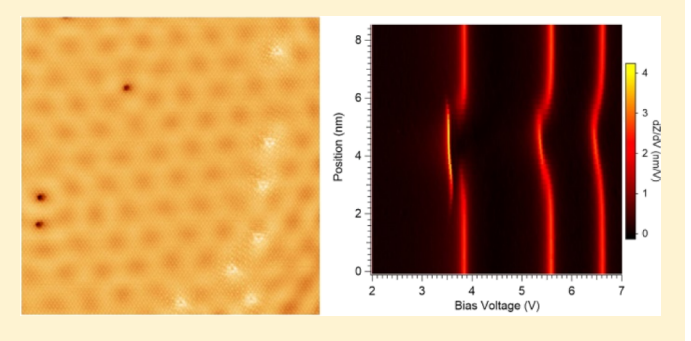


Nitrogen-Doped Graphene on Copper: Edge-Guided Doping Process and Doping-Induced Variation of Local Work Function

Joshua Neilson, Harutiun Chinkezian, Himanshu Phirke, Alexander Osei-Twumasi, Yanbang Li, Carlos Chichiri,[†] Jongweon Cho,[§] Krisztián Palotás, ^{||,⊥} Liangbing Gan, [‡] Simon J. Garrett, ^{*,‡} Kah Chun Lau,*,† and Li Gao*,†

Supporting Information

ABSTRACT: The synthesis of nitrogen-doped single-layer graphene has been achieved on the copper surface by using the nitrogen-containing sole precursor azafullerene. The synthesis process, doping properties, and doping-induced variation of local work function of graphene have been investigated on the atomic scale by combining scanning tunneling microscopy/spectroscopy, X-ray photoelectron spectroscopy measurements, and density functional theory calculations. Most nitrogen dopants are at the edges of graphene islands and the graphene domain boundaries with the pyridinic configuration. Graphitic nitrogen dopants



arrange into curved lines within graphene islands after multiple growth cycles, which results from a doping process guided by the edges of graphene islands. The doping-induced variation of local work function of the graphene surface has been measured on the atomic scale by using scanning tunneling spectroscopy measurements. We find that the local work function strongly depends on the atomic bonding configuration and concentration of nitrogen dopants. The local work function decreases for graphitic nitrogen doping but increases for pyridinic nitrogen doping. This work provides new atomic-scale insights into the synthesis of heteroatom-doped graphene from sole precursors as well as the strong correlations between nitrogen doping and the local work function of the graphene layer.

8802

1. INTRODUCTION

Graphene, the first discovered truly two-dimensional crystalline material, has demonstrated a wealth of extraordinary properties that are promising for a wide range of applications. 1-4 Substitutional doping of graphene with heteroatoms is one promising strategy for tuning the properties of graphene to realize various functions. 5,6 Nitrogen (N)doped graphene materials can potentially be used in field-effect transistors, fuel cells, solar cells, lithium-ion batteries, supercapacitors, sensors, photocatalysts, and gas storage. 5-11 The synthesis of N-doped graphene from N-containing sole precursors has recently demonstrated its feasibility with several different sole precursors. 10,12-17 A precise control of the doping properties is crucial toward the applications of doped graphene materials. By using the sole precursor azafullerene (C₅₉NH), the controlled synthesis of high-quality N-doped graphene on the ruthenium (Ru) surface has been achieved, in

which case the N-related defects exhibit a homogeneous distribution, the dopant concentration is tunable, and the primary doping configuration is pyridinic N.17 However, it remains largely unexplored how the growth substrate affects the resultant doping properties for the synthesis of heteroatomdoped graphene from sole precursors. Copper (Cu) is the most commonly used metal substrate for large-area graphene growth by chemical vapor deposition (CVD). 18 Therefore, it is of both fundamental and practical importance to investigate the synthesis of N-doped graphene on Cu using the same sole precursor C₅₉NH. The work function, which is the minimum energy required to emit an electron from the surface to vacuum, is one of the most crucial parameters for various

Received: November 20, 2018 Revised: March 12, 2019 Published: March 13, 2019



Department of Physics and Astronomy and Department of Chemistry and Biochemistry, California State University, Northridge, Northridge, California 91330, United States

^{*}Key Laboratory of Bioorganic Chemistry and Molecular Engineering of the Ministry of Education, College of Chemistry and Molecular Engineering, Peking University, Beijing 100871, China

[§]Department of Physics, Myongji University, Yongin 17058, Korea

Institute for Solid State Physics and Optics, Wigner Research Center for Physics, Hungarian Academy of Sciences, H-1525 Budapest, Hungary

[⊥]MTA-SZTE Reaction Kinetics and Surface Chemistry Research Group, University of Szeged, H-6720 Szeged, Hungary

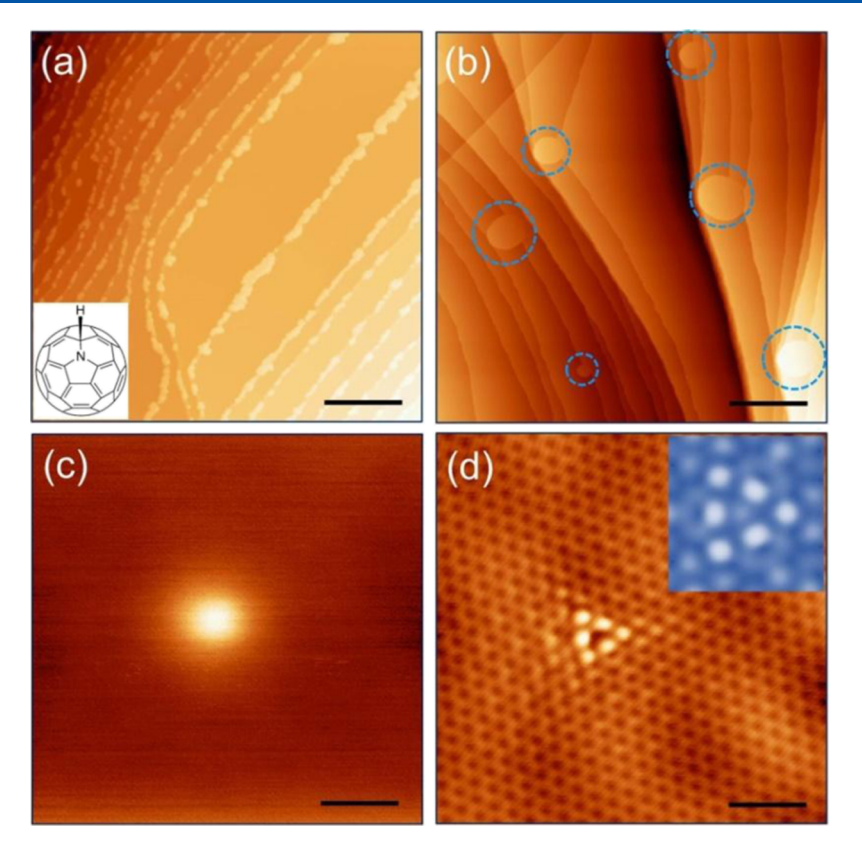


Figure 1. (a) STM image of the Cu surface covered with ~0.09 ML C_{59} NH. The inset shows the molecular structure of C_{59} NH. (b) STM image of the Cu surface after annealing the sample in (a) to 700 °C. Graphene islands are highlighted by circles. (c,d) Bias-dependent STM images of a graphitic N dopant in graphene. The inset in (d) shows a simulated STM image (1.2 nm × 1.2 nm) of a graphitic N dopant in graphene on Cu(111). The simulation was performed with a tip–sample distance of ~1.0 Å and a bias voltage of 0.1 V using Tersoff–Hamann model. Scanning parameters: (a) $V_{\text{bias}} = +2 \text{ V}$, I = 10 pA; (b) $V_{\text{bias}} = +2 \text{ V}$, I = 10 pA; (c) $V_{\text{bias}} = +1 \text{ V}$, I = 10 pA; and (d) $V_{\text{bias}} = +10 \text{ mV}$, I = 3 nA. Scale bars: (a) 40; (b) 80; (c) 1; (d) 1 nm.

practical applications of graphene including high-performance graphene-based electronic devices. 19,20 Therefore, it is also of high practical interest to investigate how the N doping impacts the local work function of graphene. Recent studies have reported that the graphitic N doping reduces the work function of graphene; ^{21–26} in particular, atomic-scale experimental studies of this effect down to an individual dopant level have been performed by measuring the local contact potential difference and the current-displacement spectra. 25,26 However, previous studies are controversial with respect to the pyridinic N doping, which decreases the work function of graphene in some studies^{22,23} but increases the work function of graphene in other studies. 21,24 Clearly, further experimental studies are needed to resolve this issue. Probing spatially resolved field emission resonances (FERs) by scanning tunneling spectroscopy (STS) is an important technique for investigating the spatial variation of local work function on surfaces. ^{27–36} This technique can also potentially be used to probe, on the atomic scale, the influence of heteroatom doping on the local work function of graphene; however, such studies are still lacking.

Here, we report the synthesis of N-doped graphene on the Cu(111) surface using the sole precursor $C_{59}NH$. The synthesis process, doping properties, and spatial variation of local work function are investigated on the atomic scale by combining scanning tunneling microscopy (STM)/STS, X-ray photoelectron spectroscopy (XPS), and density functional theory (DFT) calculations. STM/STS measurements provide

atomic-scale insights into the synthesis process, doping properties, and local work function of N-doped graphene on Cu. XPS can reveal the bonding configurations of N atoms in the graphene layer. By combining XPS and STM observations, we find that pyridinic N is the predominant doping configuration in the produced graphene layer, and a small percentage of N dopants are in graphitic N configuration. We have observed that graphitic N dopants arrange into curved lines within the graphene islands and that the number of curved lines increases with growth cycles and their shape is similar to the edges of graphene islands. STM and XPS measurements reveal that the edge of graphene islands guides the formation of these curved lines of graphitic N dopants during multiple growth cycles. The doping-induced variation of local work function of the graphene/Cu surface is measured on the atomic scale by analyzing the FERs recorded by STM. We find that the local work function decreases by 0.10 ± 0.02 eV due to single graphitic N dopant and decreases further with increasing concentration of graphitic N dopants; in contrast, the local work function increases due to pyridinic N dopants. The observed doping-induced variation of local work function is qualitatively consistent with our DFT calculations.

2. EXPERIMENTAL AND THEORETICAL METHODS

The growth experiments were performed using an ultrahigh vacuum (UHV) system with a base pressure lower than 2×10^{-10} Torr. Before being loaded into the UHV system, the Cu(111) single crystal (Princeton Scientific) was first soaked

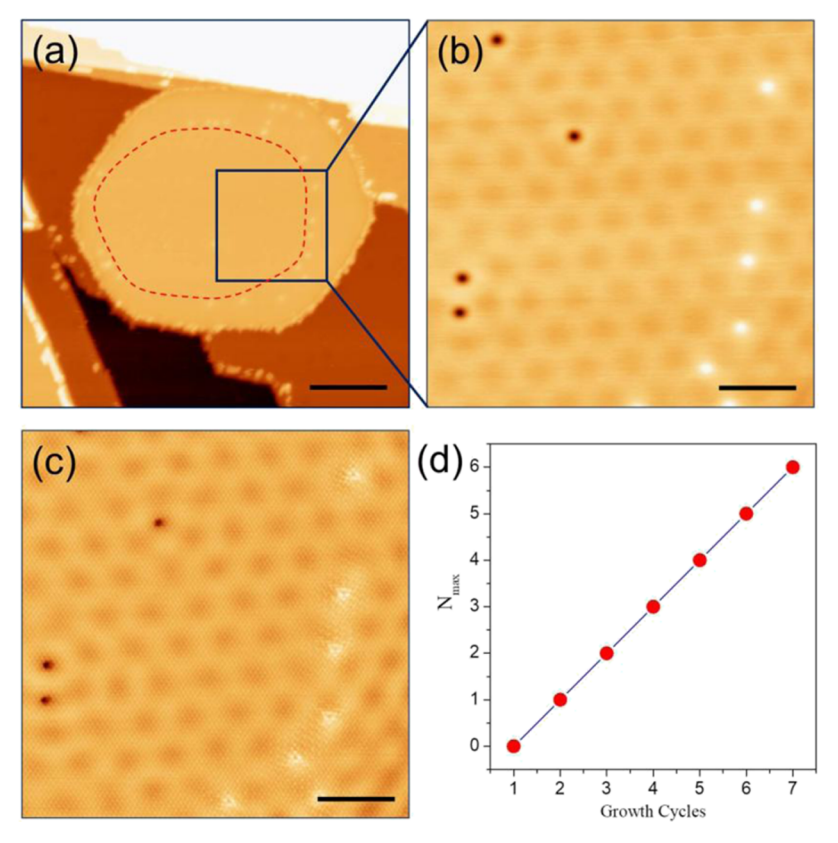


Figure 2. (a) STM image showing the curved line of bright spots (graphitic N dopants) in the graphene island. The dashed line is added as a guide. (b,c) Bias-dependent STM images of the same region highlighted in (a) showing that the curved line is composed of graphitic N dopants. (d) The maximum number of curved lines of graphitic N dopants in one graphene island as a function of growth cycles. Scanning parameters: (a) $V_{\text{bias}} = +3$ V, I = 10 pA; (b) $V_{\text{bias}} = +1$ V, I = 50 pA; and (c) $V_{\text{bias}} = +50$ mV, I = 5 nA. Scale bars: (a) 14; (b) 4; (c) 4 nm.

in a hydrochloric acid solution (1 M) for 1 h to remove the natural oxide layer and then ultrasonically cleaned in deionized water, acetone, and isopropanol. After that, the Cu(111) surface was further cleaned in UHV by repeated cycles of Ar⁺ ion sputtering (1.5 keV, 1×10^{-5} Torr, 30 min) at room temperature and subsequent thermal annealing. An anneal temperature of ~850 °C was used in the initial cycles to remove bulk impurities such as sulfur, and the anneal temperature in the subsequent cycles was in the range of 600-700 °C. The cleanness of the prepared Cu surface was checked by using STM. The C₅₉NH molecules were prepared following the procedures reported by Xin et al.³⁷ and were thoroughly degassed in UHV prior to molecular deposition. The deposition of C₅₉NH molecules was performed by thermal evaporation at \sim 330 °C from an Al₂O₃ crucible. The Cu(111) substrate was held at room temperature during molecular deposition. The growth of N-doped graphene was performed by annealing the C₅₉NH/Cu(111) sample from room temperature up to 700 °C with a step of 100 °C and a dwell time of 5 min at each temperature step.

STM and STS measurements were performed using a Unisoku UHV low-temperature STM system (USM1500S) with a base pressure lower than 2×10^{-10} Torr. All of the STM/STS measurements were carried out at 77 K with tungsten tips that were prepared by electrochemical etching and subsequently cleaned by annealing in UHV. The STM images were recorded in a constant current mode. The differential conductance (dI/dV) spectra were recorded, with the feedback loop off, by using a lock-in technique with a small ac modulation signal (853 Hz, 20 mV). The Z-V spectra were

measured by recording the tip displacement as a function of the bias voltage with a closed feedback loop and a current set point of 10 pA. The Z-V curves were numerically differentiated to obtain the dZ/dV curves. XPS measurements were performed using a Physical Electronics PHI 5200 XPS system with an Al K α X-ray source (1486.6 eV) and a hemispherical analyzer with a pass energy of 44.7 eV. The instrument was calibrated by using sputter cleaned Au [4f_{7/2} = 84.0 \pm 0.1 eV binding energy (BE)] and Cu (2p_{3/2} = 932.7 \pm 0.1 eV BE) foils

The theoretical configurations of the pristine graphene, graphitic N-doped graphene, and pyridinic N-doped graphene on Cu(111) are obtained based on geometry optimization calculations using the DFT method implemented in Vienna Ab Initio Simulation Package. 38,39 All the calculations are obtained based on the generalized gradient approximation within the Perdew-Burke-Ernzerhof method, with Grimme's D2 correction term to describe the van der Waals interaction that is present in the system. The plane wave energy cut-off was set to 500 eV, and the energy convergence criteria were set to 10^{-6} eV/atom. The force convergence limit on each atom was set to 0.01 eV/Å for the structural optimization calculations. The lattice parameters of the simulation cell are: a = b = 12.82 Å (i.e. 5 atoms along both a and b directions) and c = 25.86 Å that consists of 4 Cu(111) surface layers (i.e. 100 atoms with thickness ~6.1 Å) and a graphene layer (i.e. 54 carbon atoms). The lattice parameter on the Cu(111) surface is \sim 2.569 Å. The vacuum layer is \sim 16.75 Å. In this work, the predicted work functions of all the systems considered are based on the method proposed by Butler et al. 40 The simulated STM image is obtained based on the Tersoff–Hamann formalism that is implemented in the BSKAN code. 41,42

3. RESULTS AND DISCUSSION

3.1. Edge-Guided Doping Process. The CsoNH molecules were prepared following the procedures reported by Xin et al.,³⁷ and the molecular structure is shown in the inset of Figure 1a. A representative STM image of the Cu(111) surface is shown in Figure 1a after room-temperature deposition of ~0.09 monolayer (ML) C₅₉NH onto the surface. The molecules aggregated into islands on the terraces as well as across the step edges of the Cu surface. The molecular arrangements in the islands are not highly ordered (see Figure S1). After annealing this C₅₉NH/Cu(111) sample up to 700 °C, the C₅₉NH molecules transformed into graphene islands, as highlighted by dashed circles in Figure 1b. Differential conductance (dI/dV) measurements (see Figure S2) and atomic-resolution STM imaging (see Figure 1) verified that the obtained islands are graphene patches.⁴³ Each growth cycle includes the dosing of C₅₉NH molecules onto the Cu surface at room temperature and subsequent annealing to 700 °C. After the first growth cycle, the graphitic N dopant was observed only on very few graphene islands, while the vast majority of graphene islands are free of the graphitic N dopant. Graphitic N refers to N atoms that substitute C atoms and are sp² bonded to three atoms in the graphene lattice. Figure 1c,d shows bias-dependent STM images of a graphitic N dopant within the graphene island, which were recorded at +1 V and +10 mV, respectively. At +1 V, the graphitic N dopant is imaged as one bright spot. Atomic-resolution STM imaging of the graphitic N dopant appearing as a dip can be achieved at +10 mV, where a common interpretation is that the local density of states is strongly suppressed at the graphitic N site but greatly enhanced at the surrounding nearest six carbon sites in the other sublattice. 16,44,45 Alternative explanation supported by theoretical calculations put forward the effects of destructive quantum interference, either resulting from the electron wave functions of surface C and N atoms⁴⁶ or from s and p_z tip orbitals in the STM junction.⁴⁷ The presence of the dip above the N atom in the STM images is also confirmed in our DFT simulation of the STM image (see the inset of Figure 1d) based on Tersoff-Hamann method. 41,42 On the dI/dV spectra recorded at the point defects of the type shown in Figure 1c,d, there is no resonance at the Dirac point but a resonant state appears above the Dirac point (see Figure S3), which also suggests that this type of point defect is not a vacancy but a graphitic N. 48-50 Despite the existence of graphitic N dopants within some graphene islands after the first growth cycle, their spatial distribution is sporadic and random.

An important observation is that, after multiple growth cycles, the graphitic N dopants arrange into curved lines in the graphene islands. One of these curved lines is highlighted with the dashed line on the STM image in Figure 2a. Figure 2b,c is bias-dependent STM images of the region marked with a square on Figure 2a, recorded at +1 V and +50 mV, respectively. Such curved lines are absent on the graphene/ Cu(111) sample obtained after multiple growth cycles using the precursor C_{60} (see Figure S4). It is clear that the curved line is composed of graphitic N dopants. Atomic-resolution STM images, such as Figure 2c, indicate that the distribution of graphitic N dopants is random between the two sublattices of graphene. It is worth mentioning that the sublattice

segregation of graphitic N dopants was observed for the Ndoped graphene/Cu samples prepared by CVD from a mixture of methane, hydrogen, and ammonia or by CVD from a sole precursor pyridine. ^{16,44,51} In addition, we find that more curved lines of graphitic N appear in one graphene island with more growth cycles (see Figure S5). More interestingly, our experiments show that the maximum number of curved lines $N_{\rm max}$ in one graphene island is always one less than the number of growth cycles n, that is, $N_{\text{max}} = n - 1$, as shown in Figure 2d. After the first growth cycle, the curved line of graphitic N does not exist although there are sporadically distributed graphitic N in some graphene islands. After two growth cycles, there is one curved line of graphitic N in some graphene islands but none for the other graphene islands. After three growth cycles, there are two curved lines in some graphene islands, one curved line in some graphene islands, and none for the other islands. Basically, after multiple growth cycles, on the Cu surface, there exist graphene islands with different numbers of curved lines, and the maximum number of curved lines in one graphene island is linearly correlated with the number of growth cycles. The relation shown in Figure 2d serves as an important basis for discovering the mechanism for the formation of the observed curved lines of graphitic N. Despite recent studies on the synthesis of N-doped graphene from N-containing sole precursors, 10,12-17 this is the first-time observation of curved dopant lines in the graphene layer. We attribute the formation of the observed curved lines to an edge-guided doping process in which the N atoms are incorporated into the graphene lattice from the graphene edges during the growth process, which is to be discussed later by combining STM and XPS results.

XPS measurements have been performed to confirm the existence of N dopants and identify their bonding configurations in the graphene lattice based on the BE positions of N peaks. ^{7,10,21,24,52–56} Figure 3 shows the XPS N 1s spectra of the

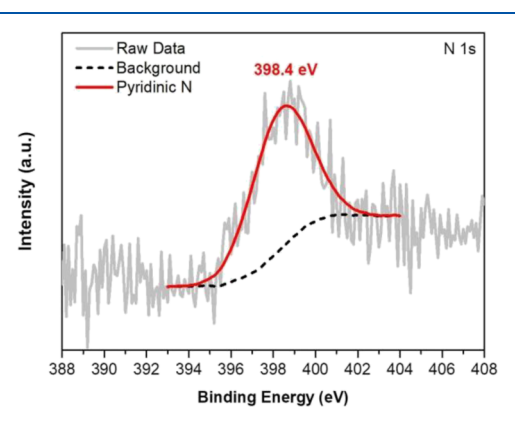


Figure 3. XPS N 1s spectra of the N-doped graphene layer on the Cu(111) surface.

synthesized N-doped single-layer graphene on the Cu(111) surface. This sample was prepared by 11 growth cycles, and the coverage of graphene is ~0.7 ML according to STM measurements. The peak at 398.4 eV BE can be attributed to pyridinic N, $^{7,10,21,24,52-56}$ which confirms that N atoms have been successfully incorporated at the edges of the graphene lattice. XPS results indicate that the predominant doping configuration is pyridinic N and the concentration of graphitic N, which is ~9 × $10^3~\mu \rm m^{-2}$ according to STM measurements, is lower than the detection limit of XPS. The concentration of

graphitic N achieved on our sample is much lower than the samples prepared by CVD or ion implantation. 14,16,44,57,58 Pyridinic N originates from sp²-hybridized N atoms bonded with two sp²-hybridized C atoms at the edges or vacancy defects in the graphene layer; therefore, the pyridinic N atoms always accompany vacancy defects or edges in the graphene layer. Within graphene islands, we did observe some vacancy defects (see Figure S6), but the amount is much less than graphitic N dopants. Therefore, the vacancy defects within graphene islands, even if they are related to pyridinic N, are not the dominant source of the observed pyridinic N peak on XPS spectra. The dominant source is most likely the N dopants at the edges of graphene islands and the graphene domain boundaries. This assignment explains the formation of dopant lines within graphene islands with increasing growth cycles, as discussed below. We scanned the edges of graphene islands and the graphene domain boundaries with the intent to resolve the atomic structure of pyridinic N dopants. The obtained atomic-resolution STM images (see Figure S7) exhibit many different features that might be related to pyridinic N, or intermediate species during the transformation from C₅₀NH to graphene, or other types of defects. We find it is difficult to identify which features on STM images correspond to pyridinic N dopants mainly because many different factors contribute to the atomic structure of edges and boundaries. Nonetheless, the pyridinic N peak on XPS spectra and the negligible amount of vacancy defects within graphene islands suggest that pyridinic N dopants predominantly exist on the edges of graphene islands and at graphene domain boundaries. It is noted that, with increasing graphene coverage, graphene islands coalesce with the formation of domain boundaries with many vacancy defects (see Figure S7). As indicated by XPS measurements (see Figure 3), the amount of pyridinic N detected by XPS is much larger than graphitic N even for a high graphene coverage (~0.7 ML), which suggests that pyridinic N dopants exist not only at the edges of graphene islands but also at the graphene domain boundaries.

Both STM and XPS measurements suggest that the edges of graphene islands play a dominant role in the formation of dopant lines. During the first growth cycle, graphene islands nucleate on the Cu surface and N atoms prefer to substitute at the edges of graphene islands with the pyridinic configuration, which has been suggested by theoretical calculations. ^{16,59} The preferential doping of heteroatoms at the edges or domain boundaries was also observed in doped graphene materials prepared by using other methods. 15,60-62 During the second growth cycle, the existing graphene islands continue to grow and, at the same time, new graphene islands nucleate on the Cu surface. When the existing islands continue to grow further, part of the pyridinic N atoms at the edges transform into graphitic N atoms in the island, leading to a line of graphitic N dopants in the island. The shape of the formed dopant lines is similar to that of the island edges. When new graphene islands nucleate, N atoms prefer to stay at the edges of islands with the pyridinic configuration and there is no line of graphitic N in the island. Therefore, after two growth cycles, some islands have a line of dopants while the others have no line of dopants. With more growth cycles, the existing graphene islands grow larger while more lines of graphitic N form in the island and, simultaneously, new graphene islands nucleate in each growth cycle. Therefore, we can identify the lower limit for the age of each graphene island by counting the number of dopant lines in the island. If the number of dopant lines is n, the island is $\geq n$

+ 1 cycles of age. We think n + 1 is the lower limit because we cannot exclude the possibility that, occasionally, none of the pyridinic N atoms transform into graphitic N while the graphene island grows during a growth cycle. For example, if n= 0, the graphene island was formed in the last growth cycle or earlier, corresponding to ≥ 1 cycles of age; if n = 1, the graphene island was formed in the cycle before last or earlier, corresponding to ≥ 2 cycles of age. The graphene islands shown in (a-f) in Figure S5 are one to six cycles of age, respectively. Although the preferential doping at the edges of graphene with heteroatoms has been observed, 21 this is the first report on the transformation from pyridinic N on the graphene edges into graphitic N within the graphene layer. The observed edge-guided doping process represents a new and important discovery for the synthesis of heteroatom-doped graphene from sole precursors.

It is interesting to note that, for the synthesis of N-doped graphene from C₅₉NH, the selection of growth substrate strongly affects the spatial distribution of N dopants in the obtained graphene layer. For the synthesis on Ru(0001), the N dopants distribute homogeneously in the graphene layer;¹⁷ however, for the synthesis on Cu(111), the N dopants in the graphene layer distribute along the curved lines due to an edgeguided doping process, as discussed above. The observed dependence of dopant distribution on the growth substrate is most likely related to the interactions between N and different growth substrates. Sforzini et al. investigated the N⁺ ion implantation of epitaxial monolayer graphene and Hintercalated quasi-freestanding monolayer graphene, both grown on 6H-SiC(0001), and found that the support of graphene has multiple influences on the N doping of the graphene layer.58

The number ratio of N and C atoms in the precursor $C_{59}NH$ is N/C=1:59, so the concentration of graphitic N would be $\sim\!6.4\times10^5~\mu\text{m}^{-2}$ if all atoms from the precursor remain on the surface and all N atoms are incorporated into the graphene lattice as graphitic N. However, the concentration of graphitic N on our sample ($\sim\!9\times10^3~\mu\text{m}^{-2}$) is much lower. Previous studies have suggested several factors that may contribute to the difference between the concentration of N dopants in graphene and the content of N in sole precursor. ^{16,17} One important factor worth mentioning here is that the formation energies for incorporating N dopants into the graphene lattice are higher than the formation energy of pristine graphene. ^{57,63}

3.2. Doping-Induced Variation of Local Work Function. To investigate how the local work function of graphene is modulated by the N doping, spatially resolved dZ/ dV measurements were performed by using STM in the voltage range from 2 to 7 V. The dZ/dV spectra exhibit a series of resonances corresponding to the Stark-shifted image potential states.⁶⁴ Because of the STM tip in close proximity to the sample surface and the resultant strong electric field, these states are often referred to as FERs which have been used to identify different metals on metal surfaces, 65 probe the spatial variation of local work function on surfaces, ²⁷⁻³⁶ and achieve atomic-resolution STM images on insulators.⁶⁶ The measurements of FERs have been used to investigate the local work function of graphene on various substrates. 30-36 This method is also desirable for probing, with high spatial resolution, the influence of heteroatom doping on the local work function of graphene; however, such studies are still lacking.

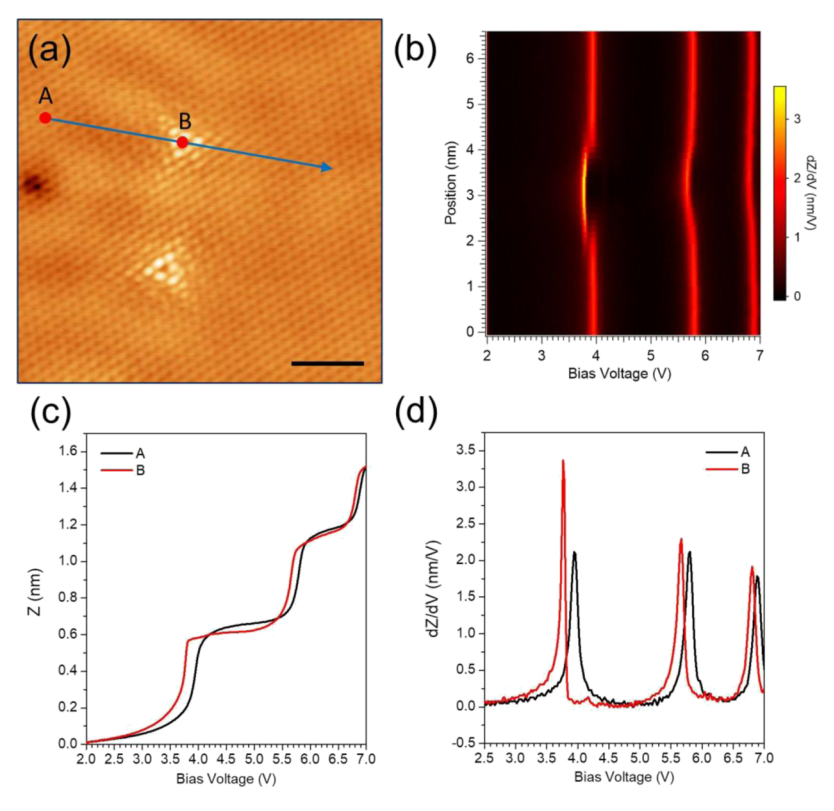


Figure 4. (a) Atomic-resolution STM image of graphitic N dopants in the graphene layer. Scanning parameters: $V_{\text{bias}} = +10 \text{ mV}$, I = 1 nA. Scale bar: 1.6 nm. (b) Two-dimensional visualization of the dZ/dV line spectra recorded along the arrowed line in (a) through a graphitic N dopant. The tunneling current remained at 10 pA for the dZ/dV line spectra measurements. (c) Z-V point spectra recorded in the pristine graphene region (A) and at the graphitic N site (B). (d) dZ/dV point spectra obtained by taking numerical differentiation of Z-V point spectra in (c).

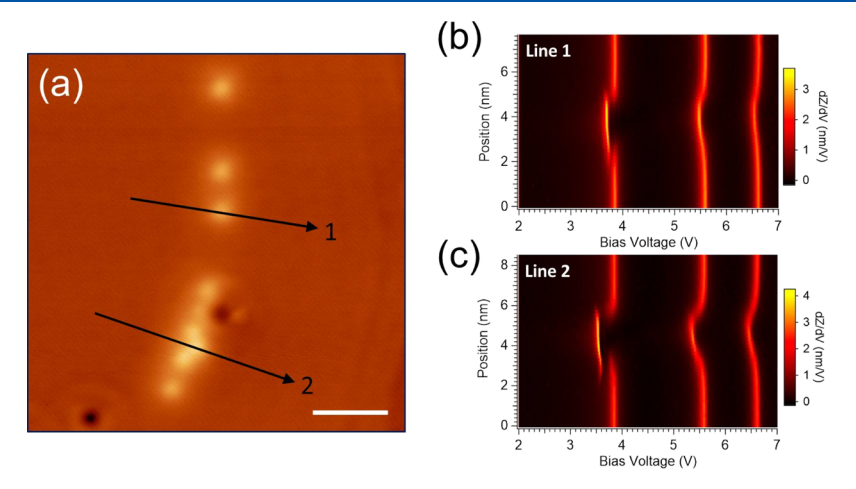


Figure 5. (a) STM image showing a curved line of graphitic N dopants. Scanning parameters: $V_{\text{bias}} = +1 \text{ V}$, I = 10 pA. Scale bar: 3 nm. (b,c) dZ/dV line spectra recorded along the line #1 and the line #2, respectively, on (a).

In order to identify the effect of graphitic N doping on the local work function, along a straight line across a single graphitic N dopant (see Figure 4a), we have measured the $\mathrm{d}Z/\mathrm{d}V$ line spectra (see Figure 4b). It is clear that the FERs shift downward in energy due to the graphitic N doping. The peak shift of FERs is not relevant to the contrast on the topography image (see Figure S8) and thus can be ascribed to the variation of local work function. The energy shift of the first FER between the low work function region and high work function region is rather sharp. At the boundaries between the two different regions, we observed the coexistence of two peaks instead of a smooth energy shift for the first FER. Such a sharp

transition of local work function was previously observed on the surface of hexagonal boron nitride on $Ir(111)^{67}$ and in the vicinity of a point defect consisting of a single adsorbed C_{60} molecule.²⁷ The energy shift becomes smoother with an increasing order of the FER, which is due to the increasing separation between the surface and higher order FER.²⁷ Figure 4c,d shows the Z-V and dZ/dV point spectra recorded at the site A and the site B, respectively, on Figure 4a. By measuring the peak shift of FERs between the graphene/Cu(111) and Cu(111) regions, we have experimentally obtained the work function of the graphene/Cu(111) surface as \sim 4.22 eV, see Figure S9. The peak position of the first FER for pristine

graphene/Cu(111) varies in the range of 3.64–3.96 eV depending on tip conditions in our measurements with 10 pA, and for each tip condition, it shifts to higher energy values with increasing current, see Figure S9. The energy shift of the second FER is approximately equal to the variation of local work function on the surface. ^{29,35,68} By analyzing the second FER of dZ/dV spectra recorded with different tip conditions, we find that the local work function of graphene decreases by 0.10 ± 0.02 eV due to a single graphitic N dopant. It is worth mentioning that different tip conditions may produce different local electric fields, which leads to different energy positions for FERs of the same order; however, the measured shift of the second FER induced by N doping remains largely unchanged with different tip conditions, as shown in Figure S11.

Figure 5 shows two dZ/dV line spectra recorded across graphitic N dopants in two different regions with different dopant concentrations (see Figure 5a). Line 1 is across a dopant in a region with a low concentration of graphitic N dopants, while line 2 is across a dopant in a region with a high concentration of graphitic N dopants. The energy shift of the second FER is 0.10 eV for line spectra #1 and 0.22 eV for line spectra #2. It is clear that the local work function of the graphene surface decreases with the increase of graphitic N dopant concentration. The dimension of the region in which the local work function is tuned by graphitic N doping increases with increasing doping concentration. For the graphitic N dopant measured by the line spectra in Figure 4b, the distance between this dopant and its nearest neighbor graphitic N dopant is ~2.9 nm. The distances are ~1.7 and ~0.6 nm for the graphitic N dopants measured by the line spectra in Figure 5b,c, respectively. From the first FER on the line spectra in Figure 4b, the dimension of the graphene region with tuned local work function is ~2.1 nm in diameter. In contrast, the corresponding dimensions are \sim 2.7 and \sim 3.1 nm, respectively, for the line spectra in Figure 5b,c. Therefore, an isolated graphitic N dopant affects its surrounding region with a diameter of ~2.1 nm, and the affected region enlarges with increasing dopant concentration.

The observed influence of graphitic N dopants on the local work function of graphene is supported by our DFT calculations. Figure 6 shows two different concentrations of

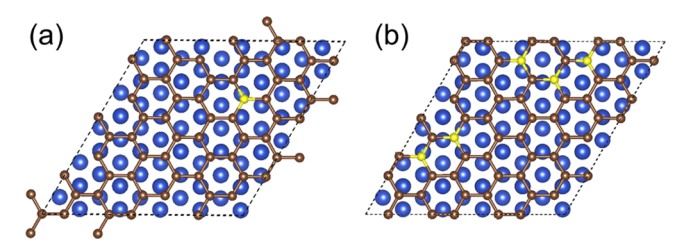


Figure 6. Two different concentrations of graphitic N used in the DFT calculations of work function for N-doped graphene on Cu(111). The Cu, C, and N atoms are in blue, brown, and yellow, respectively. The simulation cells are indicated by the dashed lines.

graphitic N dopants in graphene. The predicted work function is \sim 4.13 eV for the scenario in Figure 6a; in contrast, it is \sim 4.07 eV for the scenario in Figure 6b. The predicted work function of pristine graphene on Cu(111) is \sim 4.19 eV, which is in good agreement with the work function of \sim 4.22 eV derived from our dZ/dV measurements (see Figure S9). Therefore, our DFT calculations show that graphitic N dopants lead to the

decrease of work function of graphene, which is qualitatively consistent with our STM/STS observations.

The lifetime τ of electrons in the FER can be extracted from lifetime-broadened spectroscopic linewidths by using $\tau \approx \hbar/\Gamma$, where \hbar is the reduced Planck constant and Γ is the full width at half-maximum (FWHM) of the FERs. A Lorentzian fit was used to find the FWHM of the resonances. From the two dZ/dV point spectra in Figure 4d, the lifetimes of the first three FERs measured at site A (pristine graphene region) are \sim 4.3, ~4.6, and ~4.6 fs, respectively; however, the lifetimes of the first three FERs at site B (graphitic N site) are \sim 9.5, \sim 5.3, and ~5.3 fs, respectively. It should be noted that the lifetimes derived from dZ/dV spectra underestimate the intrinsic lifetimes of image potential states due to the broadening of the peaks induced by electric field.^{69–71} The two spectra in Figure 4d were recorded with the same tip condition and measurement parameters. Nevertheless, it is obvious that the graphitic N doping enhances the lifetimes of the FERs; and the enhancement is 5.2 fs for the first FER and 0.7 fs for the second and third FERs. The lifetime of electrons injected into a FER is limited mainly by their interaction with bulk electrons. The observed lifetime enhancement indicates that the graphitic N doping decreases the coupling of electrons in the FERs to bulk electrons, which coincides with the theoretical prediction that the N-Cu distance is slightly larger than the C-Cu distance.⁵¹

In order to identify how the local work function of graphene is affected by pyridinic N doping, dZ/dV line spectra were measured from the edge to the interior of the graphene island, as shown in Figure 7a–c. Figure 7b shows the dZ/dV point spectra recorded at A and B sites in Figure 7a. It is clear that the FERs measured at the edge shift upward in energy compared to the ones measured in the interior of the graphene island, which indicates that the local work function at the edge is higher than that in the interior of the graphene island. For the measurements in Figure 7a–c, the energy shift of the second FER is 0.21 eV. It should be noted that the increase of local work function at the graphene edge may be induced by the graphene edge itself and/or pyridinic N doping at the edge.

To further unveil the role of pyridinic N on the variation of local work function, we measured dZ/dV spectra for graphene islands on Cu(111) synthesized from C₆₀ and for the ones synthesized from C₅₉NH. For the graphene/Cu sample prepared by using C_{60} as the precursor, 72,73 there is no N dopant on the graphene edges. In contrast, by using C₅₉NH as the precursor, the graphene edges are decorated with pyridinic N dopants, as discussed above. STM images show a dark line near the edges of graphene islands on both samples, as shown in Figure 7a where the point A is on the dark line. To identify the difference in local work function between the edge and the interior of graphene islands, dZ/dV point spectra were first recorded at one randomly selected point on the dark line near the edge and then, with the same tip condition, at one selected point that is within the graphene island and 5 nm away from the first point. These two dZ/dV point spectra are called one pair of dZ/dV spectra, and the energy shift of the second FER between the two spectra in one pair is the variation of local work function between the edge and the interior of graphene islands. We performed such measurements on numerous different graphene islands with 119 pairs of dZ/dV spectra on the sample without N dopants and 110 pairs on the sample with N dopants.

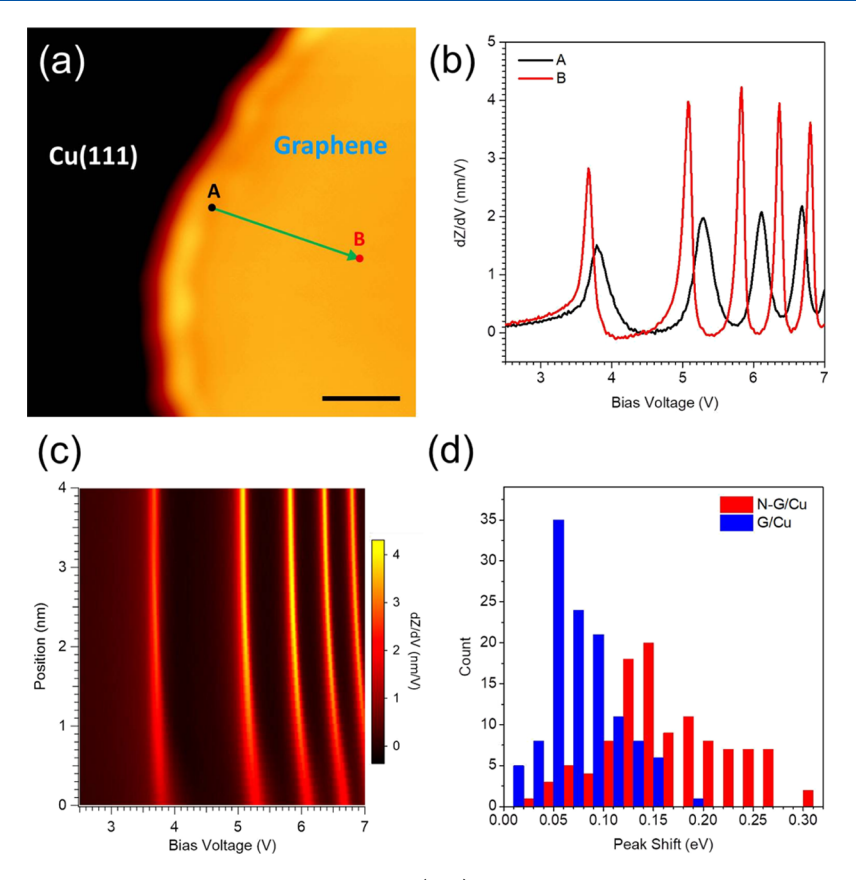


Figure 7. (a) STM image showing the edge of a graphene island on Cu(111). Scanning parameters: $V_{\text{bias}} = +2 \text{ V}$, I = 10 pA. Scale bar: 2 nm. (b) dZ/dV point spectra recorded at the two ends of the line in (a). A is near the edge of graphene island, and B is in the interior of graphene island. (c) dZ/dV line spectra recorded along the line from A to B in (a). (d) Statistics of the energy shift of the second FER between the edge and the interior of graphene islands for non-doped graphene/Cu (blue) and N-doped graphene/Cu (red). The statistics is a result of 119 and 110 pairs of dZ/dV point spectra for the non-doped and N-doped samples, respectively.

Figure 7d is the statistics of the energy shift of the second FER between the edge and the interior of graphene islands. Although different tip conditions have been used for different pairs, the peak shift values shown in Figure 7d are not related to the variation of tip conditions because the tip condition remains unchanged during the measurement of the two dZ/dVpoint spectra in each pair. Hence, the variations of peak shift values in Figure 7d reflect the variations of local work function along the edges of graphene islands on the two samples. For non-doped graphene islands, the increase of local work function at the edge relative to the interior of graphene island ranges from 0.01 to 0.18 eV, which clearly indicates that the local work function increases for non-doped graphene edges and, at the same time, varies with the atomic structure of edges. The non-uniform distribution of intermediate species on the edges leads to the variation of the atomic structure along the edges. It is interesting to note that, for N-doped graphene islands, the increase of local work function at the edge relative to the interior of graphene island ranges from 0.03 to 0.30 eV, which is obviously different from the range for non-doped graphene edges. For the N-doped graphene sample, the variation of local work function along the edges can be ascribed to the non-uniform distribution of both intermediate species and pyridinic N dopants. The statistics in Figure 7d show that overall N-doped graphene edges have higher local work function than non-doped graphene edges, which indicates that pyridinic N increases the local work function of graphene. The observed increase of local work function of graphene induced

by pyridinic N is qualitatively consistent with our DFT calculations (see Figure S12).

The doping-induced variation of local work function is caused by electron transfer. Work function is the difference between the vacuum level and the Fermi level. From our DFT calculations, the Fermi level shifts upward for graphitic N doping due to electron transfer from N to surrounding C atoms; in contrast, the Fermi level shifts downward for pyridinic N doping due to electron transfer from surrounding C atoms to N. As a result of electron transfer, the N site is positively charged for graphitic N doping but negatively charged for pyridinic N doping, as shown in Figure S13.

4. CONCLUSIONS

In summary, we have investigated the synthesis and properties of N-doped graphene on Cu(111) from the sole precursor C₅₉NH by using STM measurements, XPS measurements, and DFT calculations. We observed that graphitic N dopants arrange into curved lines within graphene islands after multiple growth cycles due to an edge-guided doping process, which is a new and important discovery for the synthesis of heteroatom-doped graphene from sole precursors. The doping-induced variation of local work function of the graphene/Cu surface has also been measured on the atomic scale by recording spatially resolved FERs with STM. The local work function decreases by 0.10 \pm 0.02 eV due to single graphitic N dopant and decreases further with increasing concentration of graphitic N dopants; in contrast, pyridinic N dopants increase local work

function. This work provides new atomic-scale insights into the process for incorporating N atoms into the graphene lattice as well as the correlations between the type of nitrogen doping and the variation of local work function, which are essential to the design, preparation, and practical applications of doped graphene materials.

ASSOCIATED CONTENT

Supporting Information

The Supporting Information is available free of charge on the ACS Publications website at DOI: 10.1021/acs.jpcc.8b11261.

STM image of the C₅₉NH molecular island on Cu(111). Differential conductance (dI/dV) line spectra across the graphene island on Cu(111) obtained after one growth cycle. dI/dV spectra recorded at the graphitic N site and in the pristine graphene region. STM images of graphene on Cu(111) after three growth cycles with the precursor C₆₀. STM images showing different numbers of curved lines of graphitic N dopants within one graphene island. STM images of different types of defects within graphene islands. STM images of the edges of graphene islands and the boundaries between different graphene domains. Comparison of dZ/dV point spectra recorded on graphitic N site, pristine graphene, and the second type of defect. The difference in local work function between the pristine graphene/Cu(111) surface and the Cu(111) surface. The shift of FERs with current for dZ/ dV spectra of the pristine graphene/Cu(111) surface measured with different tip conditions. dZ/dV point spectra recorded at the graphitic N site and in the pristine graphene region with two different tip conditions. DFT predicted work function of the graphene/Cu(111) surface with different types of N dopants. Charge density differences obtained from DFT calculations for graphitic N-defect and pyridinic Ndefect (PDF)

AUTHOR INFORMATION

Corresponding Authors

*E-mail: simon.garrett@csun.edu. Phone: 1-818-677-3366 (S.J.G.).

*E-mail: kahchun.lau@csun.edu. Phone: 1-818-677-7433 (K.C.L.).

*E-mail: li.gao@csun.edu. Phone: 1-818-677-4365 (L.G.).

ORCID ®

Jongweon Cho: 0000-0002-8956-5969 Krisztián Palotás: 0000-0002-1914-2901 Liangbing Gan: 0000-0001-6646-3452 Simon J. Garrett: 0000-0002-7710-8488 Kah Chun Lau: 0000-0002-4925-3397 Li Gao: 0000-0001-6615-6807

Notes

The authors declare no competing financial interest.

ACKNOWLEDGMENTS

We gratefully acknowledge the financial supports from National Science Foundation (NSF) (grants no. DMR-1809805 and no. DMR-1828019) and California State University Northridge. J.C. acknowledges support from Basic Science Research Program through the National Research Foundation of Korea (NRF) funded by the Ministry of Education (2017R1D1A1B03034395). K.P. acknowledges support from NRDIO-Hungary project no. FK124100.

REFERENCES

- (1) Novoselov, K. S.; Geim, A. K.; Morozov, S. V.; Jiang, D.; Zhang, Y.; Dubonos, S. V.; Grigorieva, I. V.; Firsov, A. A. Electric Field Effect in Atomically Thin Carbon Films. *Science* **2004**, *306*, 666–669.
- (2) Novoselov, K. S.; Geim, A. K.; Morozov, S. V.; Jiang, D.; Katsnelson, M. I.; Grigorieva, I. V.; Dubonos, S. V.; Firsov, A. A. Two-Dimensional Gas of Massless Dirac Fermions in Graphene. *Nature* **2005**, 438, 197–200.
- (3) Zhang, Y.; Tan, Y.-W.; Stormer, H. L.; Kim, P. Experimental Observation of the Quantum Hall Effect and Berry's Phase in Graphene. *Nature* **2005**, 438, 201–204.
- (4) Geim, A. K.; Novoselov, K. S. The Rise of Graphene. *Nat. Mater.* **2007**, *6*, 183–191.
- (5) Wang, X.; Sun, G.; Routh, P.; Kim, D.-H.; Huang, W.; Chen, P. Heteroatom-Doped Graphene Materials: Syntheses, Properties and Applications. *Chem. Soc. Rev.* **2014**, *43*, 7067–7098.
- (6) Narita, A.; Wang, X.-Y.; Feng, X.; Müllen, K. New Advances in Nanographene Chemistry. Chem. Soc. Rev. 2015, 44, 6616–6643.
- (7) Wang, H.; Maiyalagan, T.; Wang, X. Review on Recent Progress in Nitrogen-Doped Graphene: Synthesis, Characterization, and Its Potential Applications. *ACS Catal.* **2012**, *2*, 781–794.
- (8) Ito, Y.; Christodoulou, C.; Nardi, M. V.; Koch, N.; Kläui, M.; Sachdev, H.; Müllen, K. Tuning the Magnetic Properties of Carbon by Nitrogen Doping of Its Graphene Domains. *J. Am. Chem. Soc.* **2015**, 137, 7678–7685.
- (9) Shan, J.; Liu, Y.; Liu, P.; Huang, Y.; Su, Y.; Wu, D.; Feng, X. Nitrogen-Doped Carbon-Encapsulated SnO₂-SnS/Graphene Sheets with Improved Anodic Performance in Lithium Ion Batteries. *J. Mater. Chem. A* **2015**, *3*, 24148–24154.
- (10) Reddy, A. L. M.; Srivastava, A.; Gowda, S. R.; Gullapalli, H.; Dubey, M.; Ajayan, P. M. Synthesis of Nitrogen-Doped Graphene Films For Lithium Battery Application. *ACS Nano* **2010**, *4*, 6337–6342.
- (11) Yang, Z.; Nie, H.; Chen, X. A.; Chen, X.; Huang, S. Recent Progress in Doped Carbon Nanomaterials as Effective Cathode Catalysts for Fuel Cell Oxygen Reduction Reaction. *J. Power Sources* **2013**, 236, 238–249.
- (12) Jin, Z.; Yao, J.; Kittrell, C.; Tour, J. M. Large-Scale Growth and Characterizations of Nitrogen-Doped Monolayer Graphene Sheets. *ACS Nano* **2011**, *5*, 4112–4117.
- (13) Cui, T.; Lv, R.; Huang, Z.-H.; Zhu, H.; Kang, F.; Wang, K.; Wu, D. Effect of Feed Rate on the Production of Nitrogen-Doped Graphene from Liquid Acetonitrile. *Carbon* **2012**, *50*, 3659–3665.
- (14) Ito, Y.; Christodoulou, C.; Nardi, M. V.; Koch, N.; Sachdev, H.; Müllen, K. Chemical Vapor Deposition of N-Doped Graphene and Carbon Films: The Role of Precursors and Gas Phase. *ACS Nano* **2014**, *8*, 3337–3346.
- (15) Zhang, Y.; Zhang, Y.; Li, G.; Lu, J.; Lin, X.; Du, S.; Berger, R.; Feng, X.; Müllen, K.; Gao, H.-J. Direct Visualization of Atomically Precise Nitrogen-Doped Graphene Nanoribbons. *Appl. Phys. Lett.* **2014**, *105*, 023101.
- (16) Zabet-Khosousi, A.; Zhao, L.; Pálová, L.; Hybertsen, M. S.; Reichman, D. R.; Pasupathy, A. N.; Flynn, G. W. Segregation of Sublattice Domains in Nitrogen-Doped Graphene. *J. Am. Chem. Soc.* **2014**, *136*, 1391–1397.
- (17) Fei, X.; Neilson, J.; Li, Y.; Lopez, V.; Garrett, S. J.; Gan, L.; Gao, H.-J.; Gao, L. Controlled Synthesis of Nitrogen-Doped Graphene on Ruthenium from Azafullerene. *Nano Lett.* **2017**, *17*, 2887–2894.
- (18) Li, X.; Cai, W.; An, J.; Kim, S.; Nah, J.; Yang, D.; Piner, R.; Velamakanni, A.; Jung, I.; Tutuc, E.; et al. Large-Area Synthesis of High-Quality and Uniform Graphene Films on Copper Foils. *Science* **2009**, 324, 1312–1314.
- (19) Yu, Y.-J.; Zhao, Y.; Ryu, S.; Brus, L. E.; Kim, K. S.; Kim, P. Tuning the Graphene Work Function by Electric Field Effect. *Nano Lett.* **2009**, *9*, 3430–3434.

- (20) Shi, Y.; Kim, K. K.; Reina, A.; Hofmann, M.; Li, L.-J.; Kong, J. Work Function Engineering of Graphene Electrode via Chemical Doping. *ACS Nano* **2010**, *4*, 2689–2694.
- (21) Akada, K.; Terasawa, T.-o.; Imamura, G.; Obata, S.; Saiki, K. Control of Work Function of Graphene by Plasma Assisted Nitrogen Doping. *Appl. Phys. Lett.* **2014**, *104*, 131602.
- (22) Hwang, J. O.; Park, J. S.; Choi, D. S.; Kim, J. Y.; Lee, S. H.; Lee, K. E.; Kim, Y.-H.; Song, M. H.; Yoo, S.; Kim, S. O. Workfunction-Tunable, N-Doped Reduced Graphene Transparent Electrodes for High-Performance Polymer Light-Emitting Diodes. *ACS Nano* **2012**, *6*, 159–167.
- (23) Luo, Z.; Lim, S.; Tian, Z.; Shang, J.; Lai, L.; MacDonald, B.; Fu, C.; Shen, Z.; Yu, T.; Lin, J. Pyridinic N Doped Graphene: Synthesis, Electronic Structure, and Electrocatalytic Property. *J. Mater. Chem.* **2011**, 21, 8038–8044.
- (24) Schiros, T.; Nordlund, D.; Pálová, L.; Prezzi, D.; Zhao, L.; Kim, K. S.; Wurstbauer, U.; Gutiérrez, C.; Delongchamp, D.; Jaye, C.; et al. Connecting Dopant Bond Type with Electronic Structure in N-Doped Graphene. *Nano Lett.* **2012**, *12*, 4025–4031.
- (25) de la Torre, B.; Švec, M.; Hapala, P.; Redondo, J.; Krejčí, O.; Lo, R.; Manna, D.; Sarmah, A.; Nachtigallová, D.; Tuček, J.; et al. Non-Covalent Control of Spin-State in Metal-Organic Complex by Positioning on N-Doped Graphene. *Nat. Commun.* **2018**, *9*, 2831.
- (26) Telychko, M.; Mutombo, P.; Merino, P.; Hapala, P.; Ondráček, M.; Bocquet, F. C.; Sforzini, J.; Stetsovych, O.; Vondráček, M.; Jelínek, P.; et al. Electronic and Chemical Properties of Donor, Acceptor Centers in Graphene. *ACS Nano* **2015**, *9*, 9180–9187.
- (27) Ruffieux, P.; Aït-Mansour, K.; Bendounan, A.; Fasel, R.; Patthey, L.; Gröning, P.; Gröning, O. Mapping the Electronic Surface Potential of Nanostructured Surfaces. *Phys. Rev. Lett.* **2009**, *102*, 086807.
- (28) Pivetta, M.; Patthey, F.; Stengel, M.; Baldereschi, A.; Schneider, W.-D. Local Work Function Moire Pattern on Ultrathin Ionic Films: NaCl on Ag(100). *Phys. Rev. B: Condens. Matter Mater. Phys.* **2005**, 72, 115404.
- (29) Lin, C. L.; Lu, S. M.; Su, W. B.; Shih, H. T.; Wu, B. F.; Yao, Y. D.; Chang, C. S.; Tsong, T. T. Manifestation of Work Function Difference in High Order Gundlach Oscillation. *Phys. Rev. Lett.* **2007**, 99, 216103.
- (30) Feng, W.; Lei, S.; Li, Q.; Zhao, A. Periodically Modulated Electronic Properties of the Epitaxial Monolayer Graphene on Ru(0001). *J. Phys. Chem. C* **2011**, *115*, 24858–24864.
- (31) Niesner, D.; Fauster, T. Image-Potential States and Work Function of Graphene. *J. Phys.: Condens. Matter* **2014**, 26, 393001.
- (32) Borca, B.; Barja, S.; Garnica, M.; Sánchez-Portal, D.; Silkin, V. M.; Chulkov, E. V.; Hermanns, C. F.; Hinarejos, J. J.; Vázquez de Parga, A. L.; Arnau, A.; et al. Potential Energy Landscape for Hot Electrons in Periodically Nanostructured Graphene. *Phys. Rev. Lett.* **2010**, *105*, 036804.
- (33) Zhang, H. G.; Hu, H.; Pan, Y.; Mao, J. H.; Gao, M.; Guo, H. M.; Du, S. X.; Greber, T.; Gao, H.-J. Graphene Based Quantum Dots. J. Phys.: Condens. Matter 2010, 22, 302001.
- (34) Bose, S.; Silkin, V. M.; Ohmann, R.; Brihuega, I.; Vitali, L.; Michaelis, C. H.; Mallet, P.; Veuillen, J. Y.; Schneider, M. A.; Chulkov, E. V.; et al. Image Potential States as a Quantum Probe of Graphene Interfaces. *New J. Phys.* **2010**, *12*, 023028.
- (35) Craes, F.; Runte, S.; Klinkhammer, J.; Kralj, M.; Michely, T.; Busse, C. Mapping Image Potential States on Graphene Quantum Dots. *Phys. Rev. Lett.* **2013**, *111*, 056804.
- (36) Hollen, S. M.; Gambrel, G. A.; Tjung, S. J.; Santagata, N. M.; Johnston-Halperin, E.; Gupta, J. A. Modification of Electronic Surface States by Graphene Islands on Cu(111). *Phys. Rev. B: Condens. Matter Mater. Phys.* **2015**, *91*, 195425.
- (37) Xin, N.; Huang, H.; Zhang, J.; Dai, Z.; Gan, L. Fullerene Doping: Preparation of Azafullerene C_{59} NH and Oxafulleroids $C_{59}O_3$ and $C_{60}O_4$. Angew. Chem., Int. Ed. **2012**, 51, 6163–6166.
- (38) Kresse, G.; Furthmüller, J. Efficient Iterative Schemes for Ab Initio Total-Energy Calculations Using a Plane-Wave Basis Set. *Phys. Rev. B: Condens. Matter Mater. Phys.* **1996**, *54*, 11169–11186.

- (39) Kresse, G.; Furthmüller, J. Efficiency of Ab-Initio Total Energy Calculations for Metals and Semiconductors Using a Plane-Wave Basis Set. *Comput. Mater. Sci.* **1996**, *6*, 15–50.
- (40) Butler, K. T.; Hendon, C. H.; Walsh, A. Electronic Chemical Potentials of Porous Metal-Organic Frameworks. *J. Am. Chem. Soc.* **2014**, *136*, 2703–2706.
- (41) Hofer, W. A. Challenges and Errors: Interpreting High Resolution Images in Scanning Tunneling Microscopy. *Prog. Surf. Sci.* **2003**, *71*, 147–183.
- (42) Palotás, K.; Hofer, W. A. Multiple Scattering in a Vacuum Barrier Obtained from Real-Space Wavefunctions. *J. Phys.: Condens. Matter* **2005**, *17*, 2705–2713.
- (43) Gao, L.; Guest, J. R.; Guisinger, N. P. Epitaxial Graphene on Cu(111). *Nano Lett.* **2010**, *10*, 3512–3516.
- (44) Zhao, L.; He, R.; Rim, K. T.; Schiros, T.; Kim, K. S.; Zhou, H.; Gutierrez, C.; Chockalingam, S. P.; Arguello, C. J.; Palova, L.; et al. Visualizing Individual Nitrogen Dopants in Monolayer Graphene. *Science* **2011**, 333, 999–1003.
- (45) Zheng, B.; Hermet, P.; Henrard, L. Scanning Tunneling Microscopy Simulations of Nitrogen- and Boron-Doped Graphene and Single-Walled Carbon Nanotubes. *ACS Nano* **2010**, *4*, 4165–4173.
- (46) Telychko, M.; Mutombo, P.; Ondráček, M.; Hapala, P.; Bocquet, F. C.; Kolorenč, J.; Vondráček, M.; Jelínek, P.; Svec, M. Achieving High-Quality Single-Atom Nitrogen Doping of Graphene/SiC(0001) by Ion Implantation and Subsequent Thermal Stabilization. ACS Nano 2014, 8, 7318–7324.
- (47) Mándi, G.; Palotás, K. Chen's Derivative Rule Revisited: Role of Tip-Orbital Interference in STM. *Phys. Rev. B: Condens. Matter Mater. Phys.* **2015**, *91*, 165406.
- (48) Ducastelle, F. Electronic Structure of Vacancy Resonant States in Graphene: A Critical Review of the Single-Vacancy Case. *Phys. Rev. B: Condens. Matter Mater. Phys.* **2013**, *88*, 075413.
- (49) Ugeda, M. M.; Brihuega, I.; Guinea, F.; Gómez-Rodríguez, J. M. Missing Atom as a Source of Carbon Magnetism. *Phys. Rev. Lett.* **2010**, *104*, 096804.
- (50) Joucken, F.; Tison, Y.; Lagoute, J.; Dumont, J.; Cabosart, D.; Zheng, B.; Repain, V.; Chacon, C.; Girard, Y.; Botello-Méndez, A. R.; et al. Localized State and Charge Transfer in Nitrogen-Doped Graphene. *Phys. Rev. B: Condens. Matter Mater. Phys.* **2012**, 85, 161408.
- (51) Zhao, L.; Levendorf, M.; Goncher, S.; Schiros, T.; Pálová, L.; Zabet-Khosousi, A.; Rim, K. T.; Gutiérrez, C.; Nordlund, D.; Jaye, C.; et al. Local Atomic and Electronic Structure of Boron Chemical Doping in Monolayer Graphene. *Nano Lett.* **2013**, *13*, 4659–4665.
- (52) Li, X.; Wang, H.; Robinson, J. T.; Sanchez, H.; Diankov, G.; Dai, H. Simultaneous Nitrogen Doping and Reduction of Graphene Oxide. J. Am. Chem. Soc. 2009, 131, 15939–15944.
- (53) Shao, Y.; Zhang, S.; Engelhard, M. H.; Li, G.; Shao, G.; Wang, Y.; Liu, J.; Aksay, I. A.; Lin, Y. Nitrogen-Doped Graphene and Its Electrochemical Applications. *J. Mater. Chem.* **2010**, *20*, 7491–7496.
- (54) Sheng, Z.-H.; Shao, L.; Chen, J.-J.; Bao, W.-J.; Wang, F.-B.; Xia, X.-H. Catalyst-Free Synthesis of Nitrogen-Doped Graphene via Thermal Annealing Graphite Oxide with Melamine and Its Excellent Electrocatalysis. *ACS Nano* **2011**, *5*, 4350–4358.
- (55) Miao, Q.; Wang, L.; Liu, Z.; Wei, B.; Xu, F.; Fei, W. Magnetic Properties of N-Doped Graphene with High Curie Temperature. *Sci. Rep.* **2016**, *6*, 21832.
- (56) Joucken, F.; Tison, Y.; Le Fèvre, P.; Tejeda, A.; Taleb-Ibrahimi, A.; Conrad, E.; Repain, V.; Chacon, C.; Bellec, A.; Girard, Y.; et al. Charge Transfer and Electronic Doping in Nitrogen-Doped Graphene. Sci. Rep. 2015, 5, 14564.
- (57) Lv, R. T.; Li, Q.; Botello-Mendez, A. R.; Hayashi, T.; Wang, B.; Berkdemir, A.; Hao, Q. Z.; Elias, A. L.; Cruz-Silva, R.; Gutierrez, H. R.; et al. Nitrogen-Doped Graphene: Beyond Single Substitution and Enhanced Molecular Sensing. *Sci. Rep.* **2012**, *2*, 586.
- (58) Sforzini, J.; Hapala, P.; Franke, M.; van Straaten, G.; Stöhr, A.; Link, S.; Soubatch, S.; Jelínek, P.; Lee, T. L.; Starke, U.; et al.

- Structural and Electronic Properties of Nitrogen-Doped Graphene. *Phys. Rev. Lett.* **2016**, *116*, 126805.
- (59) Cruz-Silva, E.; Barnett, Z. M.; Sumpter, B. G.; Meunier, V. Structural, Magnetic, and Transport Properties of Substitutionally Doped Graphene Nanoribbons from First Principles. *Phys. Rev. B: Condens. Matter Mater. Phys.* **2011**, 83, 155445.
- (60) Jeon, I.-Y.; Choi, H. J.; Ju, M. J.; Choi, I. T.; Lim, K.; Ko, J.; Kim, H. K.; Kim, J. C.; Lee, J. J.; Shin, D.; et al. Direct Nitrogen Fixation at the Edges of Graphene Nanoplatelets as Efficient Electrocatalysts for Energy Conversion. *Sci. Rep.* **2013**, *3*, 2260.
- (61) Wang, C.; Schouteden, K.; Wu, Q.-H.; Li, Z.; Jiang, J.; Van Haesendonck, C. Atomic Resolution of Nitrogen-Doped Graphene on Cu Foils. *Nanotechnology* **2016**, *27*, 365702.
- (62) Zhang, Y.-F.; Zhang, Y.; Li, G.; Lu, J.; Que, Y.; Chen, H.; Berger, R.; Feng, X.; Müllen, K.; Lin, X.; et al. Sulfur-Doped Graphene Nanoribbons with a Sequence of Distinct Band Gaps. *Nano Res.* **2017**, 10. 3377–3384.
- (63) Yu, Y.-X. Can All Nitrogen-Doped Defects Improve the Performance of Graphene Anode Materials for Lithium-Ion Batteries? *Phys. Chem. Phys.* **2013**, *15*, 16819–16827.
- (64) Binnig, G.; Frank, K. H.; Fuchs, H.; Garcia, N.; Reihl, B.; Rohrer, H.; Salvan, F.; Williams, A. R. Tunneling Spectroscopy and Inverse Photoemission: Image and Field States. *Phys. Rev. Lett.* **1985**, 55, 991–994.
- (65) Jung, T.; Mo, Y. W.; Himpsel, F. J. Identification of Metals in Scanning Tunneling Microscopy via Image States. *Phys. Rev. Lett.* **1995**, 74, 1641–1644.
- (66) Bobrov, K.; Mayne, A. J.; Dujardin, G. Atomic-Scale Imaging of Insulating Diamond through Resonant Electron Injection. *Nature* **2001**, *413*, 616–619.
- (67) Schulz, F.; Drost, R.; Hämäläinen, S. K.; Demonchaux, T.; Seitsonen, A. P.; Liljeroth, P. Epitaxial Hexagonal Boron Nitride on Ir(111): A Work Function Template. *Phys. Rev. B: Condens. Matter Mater. Phys.* **2014**, *89*, 235429.
- (68) Wang, B.; Caffio, M.; Bromley, C.; Früchtl, H.; Schaub, R. Coupling Epitaxy, Chemical Bonding, and Work Function at the Local Scale in Transition Metal-Supported Graphene. *ACS Nano* **2010**, *4*, 5773–5782.
- (69) Pascual, J. I.; Corriol, C.; Ceballos, G.; Aldazabal, I.; Rust, H. P.; Horn, K.; Pitarke, J. M.; Echenique, P. M.; Arnau, A. Role of the Electric Field in Surface Electron Dynamics above the Vacuum Level. *Phys. Rev. B: Condens. Matter Mater. Phys.* **2007**, *75*, 165326.
- (70) Dougherty, D. B.; Maksymovych, P.; Lee, J.; Feng, M.; Petek, H.; Yates, J. T. Tunneling Spectroscopy of Stark-Shifted Image Potential States on Cu and Au Surfaces. *Phys. Rev. B: Condens. Matter Mater. Phys.* **2007**, *76*, 125428.
- (71) Crampin, S. Lifetimes of Stark-Shifted Image States. *Phys. Rev. Lett.* **2005**, 95, 046801.
- (72) Azpeitia, J.; Otero-Irurueta, G.; Palacio, I.; Martinez, J. I.; Ruiz del Arbol, N.; Santoro, G.; Gutiérrez, A.; Aballe, L.; Foerster, M.; Kalbac, M.; et al. High-Quality PVD Graphene Growth by Fullerene Decomposition on Cu Foils. *Carbon* **2017**, *119*, 535–543.
- (73) Fei, X.; Zhang, X.; Lopez, V.; Lu, G.; Gao, H.-J.; Gao, L. Strongly Interacting $C_{60}/Ir(111)$ Interface: Transformation of C_{60} into Graphene and Influence of Graphene Interlayer. *J. Phys. Chem. C* **2015**, *119*, 27550–27555.